Proceedings of the ASME 2010 3rd Joint US-European Fluids Engineering Summer Meeting and 8th International Conference on Nanochannels, Microchannels, and Minichannels
FEDSM-ICNMM2010
August 1-5, 2010, Montreal, Canada

FEDSM-ICNMM2010-30164

VISCOUS CORE-ANNULAR FLOWS IN MICROFLUIDIC CHAMBERS

Samira Darvishi **Thomas Cubaud**

Department of Mechanical Engineering, Stony Brook University
Stony Brook, New York 11794, USA
thomas.cubaud@stonybrook.edu

ABSTRACT

The manipulation of highly viscous materials at the microscale is a key challenge for implementing lab on chips with the ability to manage a variety of complex and reactive fluids. We describe methods for producing and controlling high-viscosity fluid threads flowing in sheath of less viscous fluids, i.e., viscous core-annular flows, in microchannels. The self-lubrication property of multi-fluid flows having large viscosity contrasts offers a promising means for manipulating interfaces between "thick" and "thin" fluids and for reducing the hydraulic resistance in micro- and nanofluidic devices. In particular, we focus on the flow behavior of threads as they traverse diverging-converging slit microfluidic chambers. The alteration of convective time-scales using extensional microgeometries permits the manipulation of complex phenomena such as viscous buckling, wetting, and coalescence. We examine the interrelation between these phenomena that are useful for passively enhancing mixing between miscible fluids and for initiating continuous emulsification processes between immiscible fluids having widely disparate viscosities.

INTRODUCTION

Microfluidic platforms offer great opportunities for controlling multi-fluid flows and interfaces at the small scale. The unique behavior of microflows finds applications in many fields of interests[1-3] and facilitates studies of fast reactions with reduced reagent cost and chemical waste, complex cellular processes, biomedical detection and diagnostic, environmental monitoring, as well as micro-power generation.[4-8] The manipulation of fluid interfaces is important for developing optofluidic elements, including lenses and waveguides[9-11] as well as for sequestrating reactive components into individual droplets and bubbles.[12-14] Motivated by this broad range of applications, the continuous formation of bubbles and droplets has been studied using a variety of microgeometries.[15-20]

A broad range of industrial and biological fluids are highly viscous and their manipulation at the small-scale would provide new facilities for lab-on-chip devices. Most microfluidic studies, however, have been conducted using fluids that exhibit a relatively low viscosity coefficient η. Indeed, as the dimension shrinks, the hydraulic resistance significantly increases and many of the early microflow investigations have focused on low-viscosity fluids to mitigate the large pressure drop required to displace fluids in confined microsystems. To precisely handle such fluids, a particularly promising strategy consists in the formation of a highly viscous fluid core lubricated by a less viscous fluid, i.e., a viscous core-annular flow or a viscous thread.[21-23] The self-lubrication property of fluids having a large difference in viscosities[24, 25] has been relatively unexplored in microfluidic systems. Yet, in addition to its application for fluid transport in narrow geometries, the situation of a high-viscosity fluid flowing with a low-viscosity fluid is also important for designing continuous flow-reactors between soft materials and solvents. Therefore, understanding the stability of viscous core-annular flow is essential for the development of novel microfluidic devices.

Here, we examine the behavior of viscous threads flowing in a quasi two-dimensional pore. A diverging-converging microfluidic chamber is connected with two microchannels that are square in cross-section and are used as fluid inlet and outlet. In a diverging microchannel, a viscous thread experiences a flow rate-controlled folding instability.[21] Slender viscous structures are known to buckle in a fashion similar to elastic solids during short intervals of time. In this paper, we show that the folding instability can be exploited for the interfacial control of high-viscosity fluids. Our microfluidic cell is also particularly advantageous for investigating the role of fluid properties and flow parameters in the stability of viscous core-annular flows.

First, we describe the behavior of miscible threads as this regime yields insight on the influence of the viscosity contrast between the two liquids. In particular, we describe the flow morphologies and characterize the dramatic lubrication failure of weakly diffusive threads on the top and bottom walls of the chambers. Second, we examine the behavior of core-annular flows formed between two immiscible liquids. In this situation, the differing surface energies between the liquids and the walls have a strong impact on the morphology of the fluid interfaces. As a result, the wetting properties of the thread at the walls play an important role on the flow behavior. Using different fluid pairs, we describe this system for a non-wetting thread as well as for a partially wetting thread. Novel combinations viscous and capillary instabilities are shown to offer innovative mechanisms for initiating the emulsification of a thin wetting fluid and conducting original forced wetting experiments in confined microgeometries.

MICROFLUIDIC CHAMBERS

We have fabricated hard microfluidic modules made of silicon and glass. A double-sided polished silicon wafer (h = 100 μm or 250 μm) is etched-through using DRIE and then sealed between two flat borosilicate glass plates using anodic bonding.[26] To visualize flows, the module is placed onto an inverted microscope with a fiber light on top to provide enough illumination to acquire sharp images with a high-speed camera. Fluids are injected into the channel with high-pressure syringe pumps.

Our microfluidic platform consists of two sections, a hydrodynamic focusing section to produce the thread and a square-shaped diverging-converging chamber [Fig. 1(a)]. First, a viscous thread is produced in the focusing section. The more viscous liquid ($L1$) having a viscosity η_1 is introduced in the central channel at a flow rate Q_1 and the less viscous fluid ($L2$) having a viscosity η_2 is symmetrically injected in the side channels with a total flow rate Q_2. This simple method permits the formation of a viscous core (i.e., viscous thread) made of $L1$ lubricated by the less viscous fluid $L2$ in the square microchannel that leads to the chamber. In previous studies,[21-23] we found that for large viscosity ratios $\chi = \eta_1/\eta_2 > 15$, the thread diameter normalized by the channel height, ε/h, depends only on the flow rate ratio $\varphi = Q_1/Q_2$ according to $\varepsilon/h = (\varphi/2)^{1/2}$. This scaling is useful to describe the shape of a viscous thread both in miscible environment for $Pe > 10^3$, where the Péclet number is $Pe = hV/D$ with V being the average flow velocity and D the molecular diffusion coefficient, and in immiscible surroundings when $Ca > 10^{-1}$, where the capillary number $Ca = \eta_1 V/\gamma_{12}$ and γ_{12} is the interfacial tension between $L1$ and $L2$.

Downstream from the square channel, the thread and ensheathing fluid enter the chamber that is characterized by a large width-to-height aspect ratio, w/h = 20. The large aspect ratio of the chamber allows for comparing flow behavior with a Hele-Shaw cell approximation.[27] In such a cell, a single-phase flow can be considered as irrotational and the streamlines of steady flows are expected to be identical in shape with those of

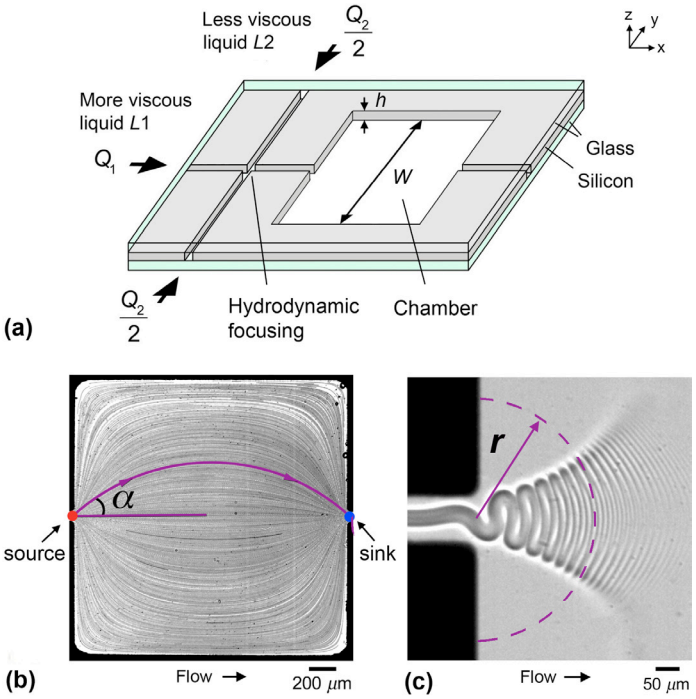

FIG. 1. Microfluidic chamber: (a) Schematic of microchannel layout, (b) single phase-flow streamlines, and (c) folding morphology at the chamber inlet.

an inviscid fluid.[28] To investigate this aspect, we have seeded the flow with 2 μm diameter spheres and superposed multiple images from a movie into a composite picture [Fig. 1(b)]. This method, which is equivalent to a long exposure photograph, allows us to describe the inlet channel flow as a source and the outlet channel as a sink. In the center of the cell, i.e., away from the sidewalls, streamlines can be roughly approximated by arc of circles and identifiable with their initial angle α. This simple analysis also suggests that, in the first section of the chamber, the mean flow velocity $V \propto 1/r$, with r being the distance from the source. Thus, material lines are expected to follow a circular shape near the chamber entrance. For instance, a thread convected in the flow field of $L2$ displays nearly circular folding lines [Fig. 1(c)].

Overall, our microfluidic chamber can be viewed as a simple fluidic component that allows for manipulating threads and high-viscosity liquids. Such flow geometry, which we have previously labeled "microfluidic aquarium,"[29] is particularly well suited for interrogating the influence of fluid properties on micro multiphase flows.

MISCIBLE VISCOUS CORE-ANNULAR FLOWS

In this section, we study miscible viscous core-annular flows. We use conventional silicone oils (i.e., polydimethylsiloxane or PDMS oils) having a wide range of viscosity: $0.82 \leq \eta \leq 5933$ cP. These polymeric oils are fully miscible and considered Newtonian in the range of shear rates γ presently investigated ($\gamma < 10^3$ s^{-1}). Provided the Péclet number is large enough, the effects of molecular diffusion are weak.

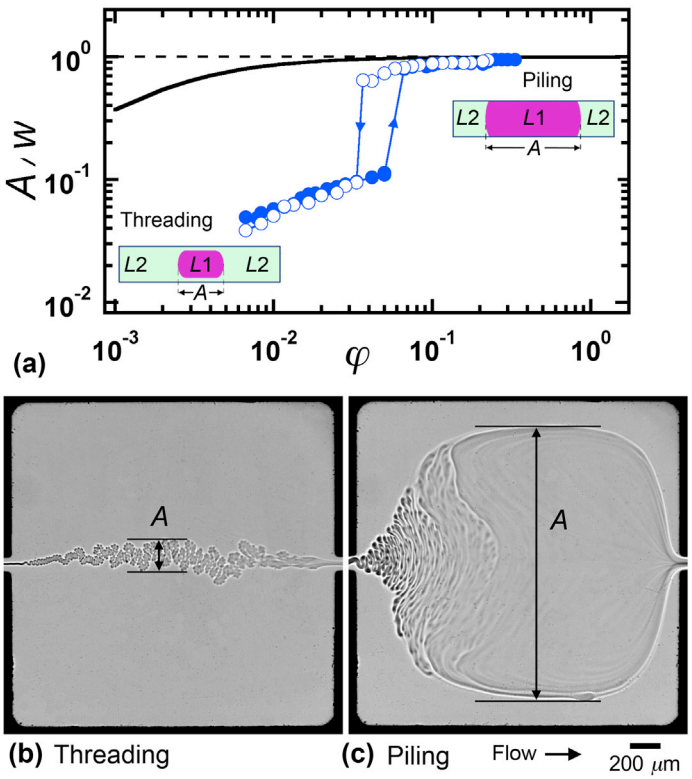

FIG. 2. Lubrication failure of a viscous thread for χ = 592. (a) Hysteresis loop between threading and piling regimes: increasing φ (●), decreasing φ (○). Solid line: $A/w = [1+(\chi\varphi)^{-1}]^{-1}$. Experimental pictures with flow rates (μl/min): (b) Q_1 = 2, Q_2 = 110; (c) Q_1 = 5, Q_2 = 40.

This system is helpful for investigating the influence of the viscosity contrast χ in the absence of the complicated effects due to interfacial tension and wetting phenomena. Since the initial thread size ε does not depends on χ nor interfacial properties in the inlet square channel, we can finely control the initial conditions and examine the role of fluid properties and flow parameters in the chamber.

The thread formed in the hydrodynamic focusing section starts to fold as it enters the chamber [Fig. 1(c)]. The folds define an envelope that typically increases in amplitude A in the first part of the chamber (diverging channel) and decreases in the second part (converging channel). Two regimes are observed: (1) small threads that can traverse the chamber while being lubricated by $L2$ at the top and bottom walls, and (2) large threads that make direct contact with the top and bottom walls. The latter situation is characteristic of a lubrication failure and we call the central region "pile" similar to parallel viscous flows.[30]

We measure the average envelope amplitude normalized by the chamber width, A/w, as a function of the flow rate ratio $\varphi = Q_1/Q_2$ [Fig. 2(a)]. For large viscosity contrasts χ, the transition between the two regimes is characterized by an abrupt variation of the amplitude A. This transition depends on the history of the system. We have investigated the hysteresis in the transition by comparing the envelope amplitude A between a system initially in the threading regime and increasing φ (i.e., increasing the initial thread diameter ε) with a system initially in the piling regime and decreasing φ (i.e., decreasing ε). Data show that near the transition the system can choose different configurations while in the well-defined thread and pile regimes, hysteresis is negligible. In this graph we have plotted the expected viscous parallel flow approximation[30] $A/w = [1+(\chi\varphi)^{-1}]^{-1}$, which asymptotically matches data for large A. Overall, hysteretic effects can alter the critical flow rate ratio for the thread lubrication failure φ_c by a factor two. This uncertainty in the transition, however, is relatively small compared to the range of variation of φ that spans over two orders of magnitude.

We have systematically conducted experiments using a variety of viscosity contrasts χ [Fig. 3]. For clarity, we show only data when the thread decreases in size and for large Péclet numbers ($Pe > 10^3$) to focus on the behavior of weakly diffusive threads. Indeed, for small flow rates, molecular diffusion blurs the interface and can also significantly alter the transition. As the viscosity contrast χ decreases, the lubrication transition becomes smoother and occurs at a larger flow rate φ. This behavior is related to the ability of a thread to bend in a viscous environment. In general, as the viscosity contrast increases, the thread folding amplitude increases. The smooth transition at low χ is due to a partial lubrication failure. Indeed, the system can readily integrate the two states (threading and piling) for low χ because the thread is relatively less viscous and therefore can "reflow" in the pile. For comparison, we plot the Hele-Shaw cell approximation for χ = 1: $A/w = [1+\varphi^{-1}]^{-1}$, which corresponds to the upper limit in φ. Overall, upon carefully examining the transition for numerous flow rates and viscosity contrasts, we define the lubrication transition to occur when $A/w \approx 0.3$, which given our channel geometry (w/h = 20) corresponds to $A \approx 6h$.

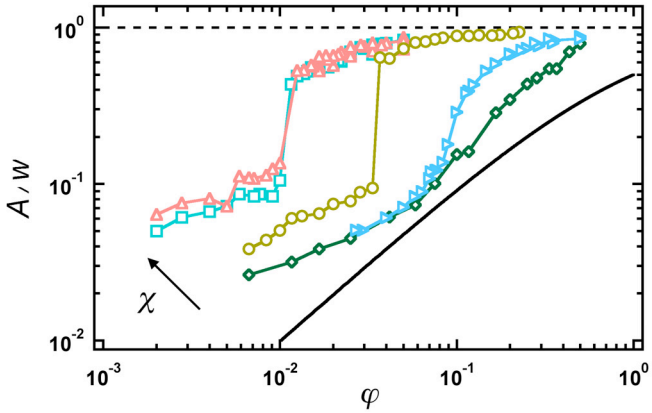

FIG.3. Evolution of the amplitude A for χ = 52 (◇), 106 (▷), 592 (○), 2796 (□), and 5933 (△). Solid line: $A/w = [1+\varphi^{-1}]^{-1}$.

We measure the flow rate ratio φ_c corresponding to the lubrication transition (i.e., when $A/w \approx 0.3$) for a broad range of viscosity contrasts χ [Fig. 4(a)]. Although for each χ, the transition can vary due to the complex interplay between folding and diffusion, experiments show that φ_c decreases with χ. We fit our data with a power law and find that the function $\varphi_c = 1.8\chi^{-0.62}$ compares well with experimental behavior. Here, the coefficient -0.62 is very close to -2/3 and this simple functional relationship is useful for predicting the lubrication failure of a viscous thread in a chamber as a function of χ. In particular, by relating φ and ε, we conclude that the critical initial size ε_c for a thread to traverse the chamber without piling decreases with the viscosity contrast χ.

We have also examined the influence of χ on the threading regime. Since the diameter of a lubricated thread in a square channel follows $\varepsilon/h = (\varphi/2)^{1/2}$, by extension, we fit the amplitude of a lubricated folded thread in the chamber with $A/w = k\varphi^{1/2}$. The prefactor k is a function of the viscosity contrast χ as can be seen in Fig. 4(b). Data are reasonably well fit by the function $k = 0.06\chi^{0.35}$, which yields the estimate $A/w \approx c\chi^{1/3}\varphi^{1/2}$ with $c = 0.06$. This result shows that although folding morphologies are rather intricate, the mean behavior of the system can be described using basic scaling laws.

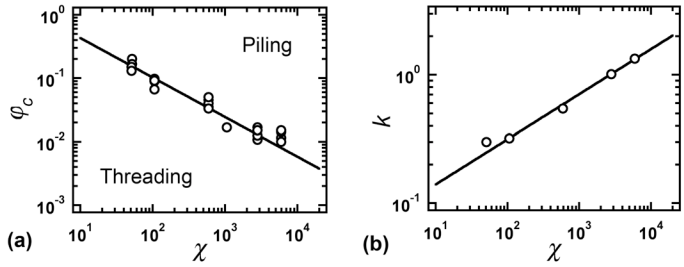

FIG. 4. Influence of viscosity contrast χ. (a) Critical flow rate ratio φ_c for lubrication transition. Solid line: $\varphi_c = 1.8\chi^{-0.62}$. (b) Evolution of the prefactor k. Solid line: $k = 0.06\chi^{0.35}$

We now study the folding morphologies in the chamber. Two parameters are introduced to quantify the shape of the more viscous central layer. The first criterion is the penetration length X_P of the lubricated thread into the pile. Indeed, at the chamber entrance, the thread is lubricated and deposits $L1$ into the slow moving pile. The location of this transition can be estimated from experimental micrographs by examining the regions where folds start to disappear into the pile. This transition also corresponds to the inversion of the envelope curvature of the central stream [Fig. 5]. Thus, when $X_P/w = 1$, the thread remains lubricated along the chamber. Smaller penetration length $X_P/w < 1$ indicates that the pile is formed. For low χ, we systematically observe that the pile forms near the end of the chamber. Increasing the flow rate ratio φ results in a pile formation in the upstream direction. The assumption that X_P/w decreases with φ is confirmed experimentally [Fig. 5(a)].

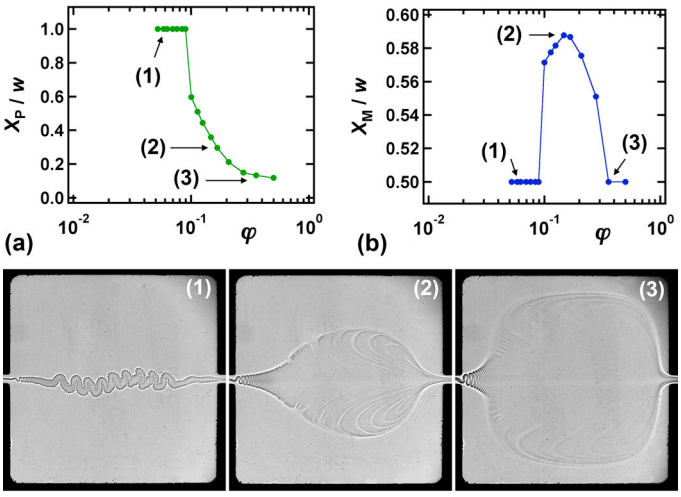

FIG. 5. Morphological features of folding threads (χ = 52). (a) Apparent penetration length of lubrication X_P/w as a function of flow rate ratio φ. (b) Location of maximum amplitude X_M/w for various φ. Bottom: corresponding experimental micrographs (h = 100 μm, flow rates in μl/min): (1) Q_1 = 10, Q_2 = 180, (2) Q_1 = 7, Q_2 = 40, (3) Q_1 = 5, Q_2 = 14.

The second criterion is the location of the maximum central stream amplitude X_M. The lubrication failure is associated with an increase of the amplitude A to conserve mass due to the decrease in the stream velocity resulting from the contact of the more viscous liquid $L1$ with the walls. Therefore, the location of the maximum amplitude X_M indicates where the center of the pile is positioned. For a lubricated thread, the maximum is expected in the center of the chamber $X_M/w = 0.5$ according to the single-phase streamlines. Similarly, the center of a fully formed pile is expected in the chamber center. During the transition, however, X_M appears to shift toward the chamber outlet as displayed Fig. 5(b). Our two parameters, X_P and X_M, are useful indicators of the smooth the lubrication transition for low χ.

IMMISCIBLE VISCOUS CORE-ANNULAR FLOWS

In this section, we investigate the behavior of immiscible viscous core-annular flows in microfluidic chambers. The wetting and interfacial tension properties of the fluids play a major role in the flow structure. Indeed, the stability of the thin lubricating film of $L2$ between the thread and the walls is strongly affected by the intermolecular forces between the solid walls and the fluids. These interactions determine the contact angle θ_{12}, which we define with respect to the fluid thread. While wetting is important for the film stability, the interfacial tension γ_{12} between $L1$ and $L2$ alters the buckling morphologies. The overall effect of interfacial tension is to reduce the thread specific surface area. By contrast with the miscible fluids case, in a microfluidic chamber, immiscible fluids can be emulsified and forced wetting behaviors investigated.

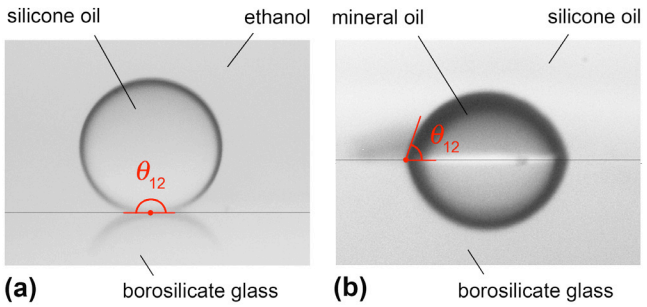

FIG. 6. Contact angle measurement on borosilicate glass. (a) *L*1: silicone oil, *L*2: ethanol, $\theta_{12} \approx 180^{o}$. (b) *L*1: Heavy mineral oil, *L*2: silicone oil, $\theta_{12} \approx 70$. Droplets are reflected on the glass surface.

We examine microflows in two situations: (a) for a non-wetting thread and (b) for a partially wetting thread. Fluid pairs were selected according to their mutual contact angle on borosilicate glass. For the non-wetting case, we used a silicone oil having a viscosity $\eta_1 = 485$ cP for $L1$ and ethanol for $L2$ ($\eta_2 = 1.16$ cP). The contact angle in this situation approaches $\theta_{12} \approx 180^{\circ}$ and a drop of $L1$ in a continuous phase of $L2$ assumes the typical bead shape [Fig. 6(a)]. Using the double capillary rise method[31] in well-characterized borosilicate glass tubes, we measure the interfacial tension $\gamma_{12} = 1.7$ mN/m between $L1$ and $L2$. For the wetting case, we use a heavy mineral oil having a viscosity $\eta_1 = 131$ cP for $L1$ and a silicone oil having a viscosity $\eta_2 = 6.5$ cP for $L2$. The contact angle in this case is $\theta_{12} \approx 70^{\circ}$ [Fig. 6(b)], which is less than $\pi/2$. Hence, the mineral oil wets the hydrophilic glass walls more than the silicone oil. The determination of interfacial tension in a partially wetting situation is difficult due to contact angle hysteresis. Using the double capillary rise method in conjunction with contact angle measurements, we estimate the interfacial tension $\gamma_{12} \approx 10$ mN/m for the mineral/silicone oils fluid pair.

Non-wetting thread

For the case of a non-wetting thread (where $L1$ is made of silicone oil and $L2$ is made of ethanol, contact angle $\theta_{12} \approx 180^{o}$, viscosity contrast $\chi = 419$), we observe an intriguing mechanism of droplet formation between the pile and the walls. Although, in this system, the complete wetting of the solid walls by $L2$ prevents the film from rupturing (i.e., dewetting), the folding instability produces local variations in the film thickness δ that induce film rearrangement and ultimately produce droplets. Indeed, at the entrance region of the chamber, folds are compacted and coalesce to form the pile. The $L2$ film thickness δ between the walls and the $L1$ pile is larger along each fold coalescence line. The curvature of the $L1/L2$ interface gives rise to a local capillary pressure gradient in the film that drains $L2$ toward the wedge formed by each coalescence line. The combined effect of the average decrease of δ along the flow direction and the local $L1/L2$ curvature leads to the formation of droplets along each coalescence line [Fig. 7]. This

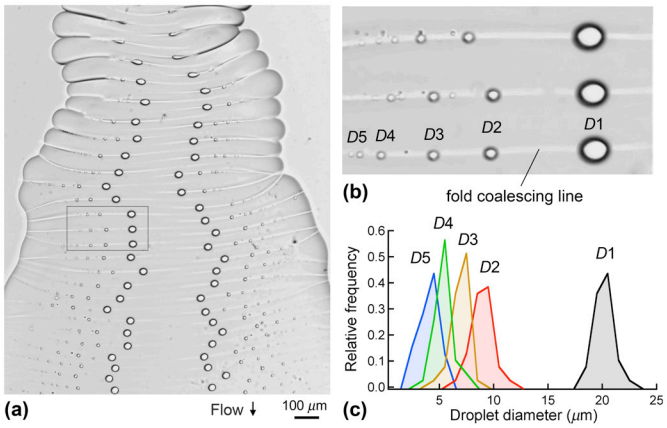

FIG. 7. Droplet decorated stream. (a) Experimental micrograph, $h = 250$ μm, flow rates in μl/min: $Q_1 = 120$, $Q_2 = 240$. (b) Magnified view of the pile showing droplet arrays along fold coalescence lines. (c) Droplet size distribution in the pile.

mechanism is somehow analogous to dry foam behavior where liquid is collected into plateau borders and vertex due to interfacial curvature.[32,33]

Overall, this emergent phenomenon can produce regular assembly of multi-scale droplets. The flow pattern is characterized by arrays of transverse fold coalescence lines with large droplets $D1$ forming near the center of the pile. Along each coalescence line, we also observe a succession of smaller droplets $D2$, $D3$, etc., the size of which continuously decreases toward the pile edge. Therefore, the pile morphology appears with two large droplets near the center and smaller droplets near the edges. Following the flow history, primary droplets $D1$ are formed first and represent the largest volume of $L2$. We have measured the droplet size distribution along the 40 bottom fold lines for the case displayed in Fig. 7. We find that the size distribution is relatively narrow for each droplet category. Indeed, for the primary droplets $D1$, we obtain $d_1 = 20 \pm 2$ μm, and for the secondary droplets $D2$, we find $d_2 = 9 \pm 2$ μm. Other droplets sizes are $d_3 = 7 \pm 2$ μm, $d_4 = 5 \pm 2$ μm, $d_5 = 4 \pm 2$ μm. The formation of "droplet-decorated" streams is of fundamental interest since it permits the regular generation of droplets having sizes ($d \leq 20$ μm) that are at least one order of magnitude smaller than the channel height ($h = 250$ μm).

Partially wetting thread

In the situation of a partially wetting thread (where $L1$ is made of heavy mineral oil and $L2$ is made of silicone oil, contact angle $\theta_{12} \approx 70^{o}$, viscosity contrast $\chi = 20$), we observe a variety of forced wetting phenomena during the thread lubrication transition in the cell. This system offers the possibility to examine the competing effects between wetting and encapsulation mechanisms. Indeed, although the large viscosity contrast χ between the fluids facilitates the ensheathing of $L1$ with the formation of a lubricating layer of $L2$ at the walls, the

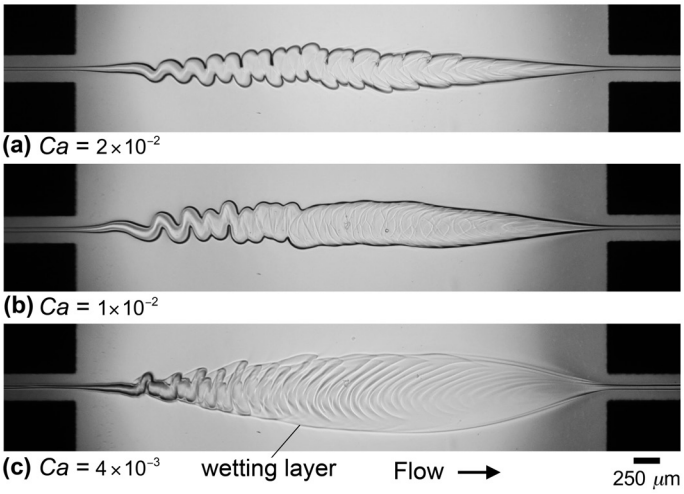

FIG. 8. Influence of capillary number *Ca* and wetting transition for fixed flow rate ratio: $\varphi = 5 \times 10^{-2}$. Flow rates in μl/min: (a) $Q_1 = 5$, $Q_2 = 100$, $Ca = 2 \times 10^{-2}$; (b) $Q_1 = 2.5$, $Q_2 = 50$, $Ca = 10^{-2}$; (c) $Q_1 = 1$, $Q_2 = 20$, $Ca = 4 \times 10^{-3}$.

preferred adhesion of $L1$ at the walls can potentially substitute the $L2$ lubricating layer by a $L1$ wetting layer.

An important aspect of wetting phenomena is rooted in the evolution of the dynamic contact angle θ as a function of the capillary number Ca. For a given fluid pair, it is well known that the advancing contact angle θ_A increases with the contact line velocity while the receding contact angle θ_R decreases.[34,35] Hence, a dynamic wetting transition occurs above a critical capillary number $Ca_c \approx 10^{-2}$ as $\theta_A \rightarrow \pi$ and θ_R becomes null.[22] Our microfluidic system, which is composed of a square microchannel with an average velocity $V_{square} = (Q_1+Q_2)/h^2$ followed by a plane chamber with an average velocity $V_{chamber} = (Q_1+Q_2)/(hw)$, allows for investigating the crossover between wetting and lubricating regimes. The large reduction in the flow speed between the chamber and the square channel, $V_{chamber} = V_{square}/20$, is exploited to locally initiate wetting phenomena when $Ca_{chamber} < 10^{-2}$ while these effects are not present in the square microchannel when $Ca_{square} > 10^{-1}$. In other words, the dynamic wetting transition in the chamber can be controlled with the flow rates.

The influence of the capillary number Ca on the chamber flow morphology is shown in Fig. 8. For low Ca, the combined effect of wetting and interfacial tension causes the thread $L1$ to adhere to the walls due to the favorable surface energy. This effect results in the relatively large envelope amplitude A. For larger Ca, viscous effects dominate capillary effects and overall favor the formation of a lubricating layer between the thread and the walls. As the capillary number Ca increases, the folding patterns become more persistent.

We measure the evolution of the normalized thread amplitude A/w as a function of the flow rate ratio φ [Fig. 9]. In this series of experiments, we have fixed the side flow rate Q_2 and progressively increased the thread flow rate Q_1 to

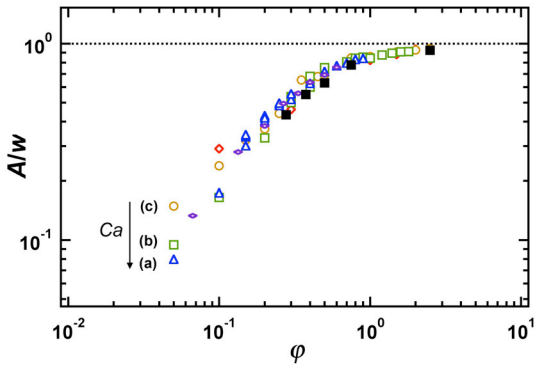

FIG. 9. Evolution of the normalized envelope amplitude *A*/*w* as a function of the flow rate ratio φ for various fixed side flow rate (in μl/min) $Q_2 = 10$ (◇), 20 (○), 50 (□), 100 (△), 150 (▷). (a), (b), and (c) correspond to data in Fig. 8.

investigate the transition from a thread to a pile. The relatively smooth relationship between A and φ is expected given the small viscosity contrast $\chi = 20$ between the fluids. We note that for small and lubricated threads, the amplitude decreases with Ca as explained above. By contrast, larger threads readily make direct contact with the walls. The lubrication failure reduces the $L1/L2$ interfacial area and overall the pile amplitude becomes independent from the capillary number Ca.

We now focus on the pile morphology for low capillary number flows [Fig. 10]. This partially wetting system is

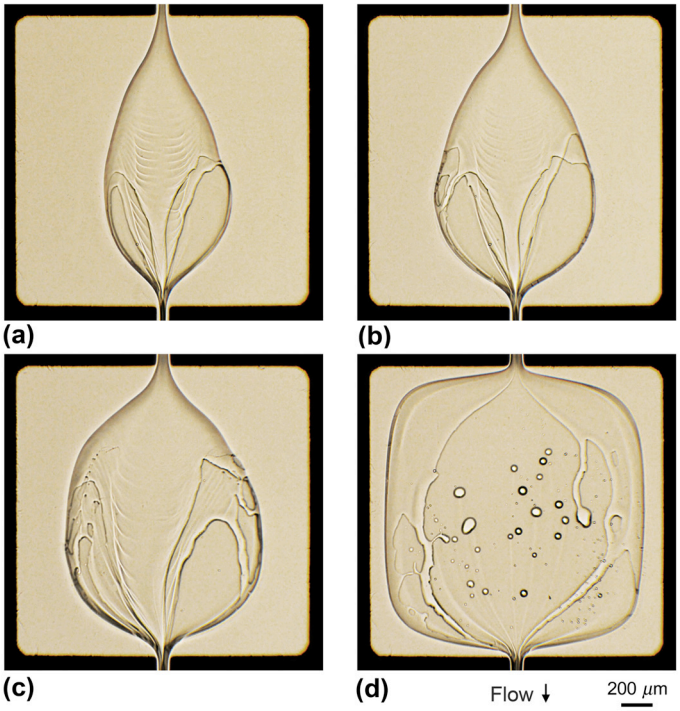

FIG. 10. Dewetting flow patterns. Flow rates in μl/min. (a) $Q_1 = 1.5$, $Q_2 = 5.4$, $\varphi = 0.28$, $Ca = 7.5 \times 10^{-3}$; (b) $Q_1 = 1.5$, $Q_2 = 4$, $\varphi = 0.37$, $Ca = 6 \times 10^{-3}$; (c) $Q_1 = 1.5$, $Q_2 = 3$, $\varphi = 0.5$, $Ca = 4.9 \times 10^{-3}$; (d) $Q_1 = 5$, $Q_2 = 2$, $\varphi = 2.5$, $Ca = 7.6 \times 10^{-3}$

advantageous for examining the thin film stability since contact lines are clearly identifiable on the micrographs. In this series of experiments, interfacial phenomena largely dominate viscous effects, which results in the apparent damping of the folding instability. Although the thread oscillations are significantly reduced, the small variations in the $L2$ film thickness δ are present and develop downstream into small ripples [Fig. 10(a)]. The main feature of this regime is the formation and growth of dewetting patches. The interaction between contact angle hysteresis and multi-fluid flow in the chamber can lead to the formation of pinned contact lines. In these photographs, we visualize contact lines forming both at the top and at the bottom walls. The nucleation sites of the dewetting patches are located in the slow moving regions of the pile, i.e., in the second half of the chamber near the pile edges. In the absence of external flow, a dewetting patch grows circularly on an homogeneous surface by collecting liquid in a rim rear the contact lines.[36] Here, the external flow significantly distorts the patches. Growth of $L1$ patches at the walls is facilitated by the flow in downstream patch regions while it is hindered in the upstream patch regions since, in this area, the patch growth against the flow direction. As a result, the system displays the typical morphologies of dewetting arches similar to macro-scale systems.[37] For intermediate pile amplitude A, since contact lines have a tendency to align with the flow, we observe the formation of rivulets (i.e., continuous fingers) in the central region. For larger A, most of the pile is dewetted [Fig. 10(d)] and droplets of $L2$ can stick to the walls in the center of the pile. This phenomenon is closely related with the stability of the rivulet that can break into an assembly of droplets when not "fed" by $L2$.

For larger capillary numbers Ca, the system is characterized by a periodical succession of lubrication and dewetted states. Future investigations will focus on the quantification of the wetted area as a function of flow parameters and fluid thermophysical properties. The fluid pair mineral/silicone oil is advantageous to initiate this type of forced wetting phenomena.

CONCLUSION

In this paper, we have characterized the lubrication failure of viscous threads both in miscible and immiscible environments using a microfluidic chamber. The single-phase flow streamlines in our a quasi two-dimensional cell can be approximated by arc of circles in the center of the chamber. We showed that weakly diffusive viscous core-annular flows experience a dramatic lubrication failure as a function of the flow rates Q_1 and Q_2 and the viscosity contrast $\chi = \eta_1/\eta_2$. We found a simple estimate for the critical flow rate ratio φ_c as a function of χ that enables the prediction of the transition. In addition, we have characterized the amplitude of the folding envelope in the threading regime and we have introduced geometric parameters for analyzing the pile morphology. When fluids are immiscible, we have studied the behavior of capillary threads in the non-wetting and partially wetting cases. In summary, a non-wetting thread can be used to emulsify the less viscous fluid layer at the walls and produce intriguing "droplet-decorated" streams composed of arrays of multi-scale droplets, the size of which is at least one order of magnitude smaller than the chamber smallest dimension h. A partially wetting exhibits a complex behavior depending on contact hysteresis. A regime of a particular interest corresponds to the formation and growth of dewetting patches between the liquids and the walls.

Although much interest has been given to the formation of droplets and bubbles in microfluidics, better understanding core-annular flow regimes yields insight into novel flow configurations of both fundamental and practical interests. Here we have investigated the degree of deformation that such structure can sustain in a two-dimensional cell primarily as a function of the viscosity contrast. Future studies will focus on the quantification of the film thickness δ at the walls in both miscible and immiscible cases. The systematic variation of the contact angle between a capillary thread and the walls is expected to shed new light onto the complex interplay between thread encapsulation and wetting properties. Controlling the lubrication of fluids having a large difference in viscosity is pivotal for the development of novel microflow reactors for soft materials.

ACKNOWLEDGMENTS

This work was supported by NSF grant CBET-0932925.

REFERENCES

1. C.-M. Ho and Y.-C. Tai, "Micro-electro-mechanical systems (MEMS) and fluid flows," *Annu. Rev. Fluid Mech.* **30**, 579-612 (1998).
2. H. A. Stone, A. D. Stroock and A. Ajdari, "Engineering flows in small devices: microfluidics toward a lab-on-a-chip," *Annu. Rev. Fluid Mech.* **2004**, 381-411 (2004).
3. T. M. Squires and S. R. Quake, "Microfluidics: fluid physics at the nanoliter scale," *Rev. Mod. Phys.* **77**, 977-1026 (2005).
4. P. Yager, T. Edwards, E. GFu, K. Helton, K. Nelson, M. R. Tam and B. H. Weigl, "Mirofluidic diagnostic technologies for global public health," *Nature (London)* **442**, 412-418 (2006).
5. A. J. deMello, "Control and detection of chemical reactions in microfluidic systems," *Nature (London)* **442**, 394-402 (2006).
6. J. El-Ali, P. K. Sorger and K. F. Jensen, "Cells on chips," *Nature (London)* **442**, 403-411 (2006).
7. H. Craighead, "Future lab-on-chip technologies for interogating individual molecules," *Nature (London)* **442**, 387-393 (2006).
8. D. D. Meng, T. Cubaud, C.-M. Ho and C.-J. Kim, "A methanol-tolerant gas-venting microchannel for microdirect methanol fuel cell," *J. Microelectromechanical Systems* **16**, 1403-1410 (2007).
9. D. B. Wolfe, R. S. Conroy, P. Garstecki, B. T. Mayer, M. A. Fischbach, K. E. Paul, M. Prentiss and G. M. Whitesides, "Dynamic control of liquid-core/liquid-cladding optical waveguides," *Proc. Nat. Acad. Sci.* **101**, 12434-12438 (2004).
10. X. Mao, J. R. Waldeisen, B. K. Juluri and T. H. Huang, "Hydrodynamically tunable optofluidic cylindrical microlens," *Lab Chip* **7**, 1303-1308 (2007).
11. S. K. Y. Tang, C. A. Stan and G. M. Whitesides, "Dynamically reconfigurable liquid-core liquid-cladding lens in a microfluidic channel," *Lab Chip* **8**, 394-401 (2008).

12. H. Song, D. L. Chen and R. F. Ismagilov, "Reactions in droplets in microfluidic channels," *Andew. Chem. Int. Ed.* **45**, 7336-7356 (2006).
13. S. Y. Teh, R. Lin, L. H. Hung and A. P. Lee, "Droplet microfluidics," *Lab Chip* **8**, 198-220 (2008).
14. A. Günther and K. F. Jensen, "Multiphase microfluidic: from flow characteristics to chemical and material synthesis," *Lab Chip* **6**, 1487-1503 (2006).
15. T. Kawakatsu, H. Komori, M. Nakajima, Y. Kikuchi and T. Yonemoto, "Production of monodisperse oil-in-water emulsion using cross flow-type silicon microchannel plate," *J. Chem. Eng. Japan* **32**, 241-244 (1999).
16. S. L. Anna, N. Bontoux and H. A. Stone, "Formation of dispersions using "flow focusing" in microchannels," *App. Phys. Lett.* **82**, 364-366 (2003).
17. Q. Xu and M. Nakajima, "The generation of highly monodisperse droplets through the breakup of hydrodynamically focused microthread in a microfluidic device," *App. Phys. Lett.* **85**, 3726-3728 (2004).
18. T. Cubaud, M. Tatineni, X. Zhong and C.-M. Ho, "Bubble dispenser in microfluidic devices," *Phys. Rev. E* **72**, 037302 (2005).
19. P. Garstecki, M. Fuerstman, H. A. Stone and G. W. Whitesides, "Formation of droplets and bubbles in a microfluidic T-junction-scaling and mechanism of breakup," *Lab Chip* **6**, 437-446 (2006).
20. A. S. Utada, A. Fernandez-Nieves, H. A. Stone and D. A. Weitz, "Dripping to jetting transitions in coflowing liquid streams," *Phys. Rev. Lett.* **99**, 094502 (2007).
21. T. Cubaud and T. G. Mason, "Folding of viscous threads in diverging microchannels," *Phys. Rev. Lett.* **96**, 114501 (2006).
22. T. Cubaud and T. G. Mason, "Capillary threads and viscous droplets in square microchannels," *Phys. Fluids* **20**, 053302 (2008).
23. T. Cubaud and T. G. Mason, "High-viscosity fluid threads in weakly diffusive microfluidic systems," *New J. Phys.* **11**, 075029 (2009).
24. D. D. Joseph, K. Nguyen and G. S. Beavers, "Non-uniqueness and stability of the configuration of flow of immiscible fluids with different viscosities," *J. Fluid Mech.* **141**, 319-345 (1984).
25. D. D. Joseph and Y. Y. Renardy, "Fundamentals of Two-Fluid Dynamics. Part II: Lubricated Transport, Drops and Miscible Liquids " Springer-Verlag, New York (1993).
26. T. Cubaud and C.-M. Ho, "Transport of bubbles in square microchannels," *Phys. Fluids* **16**, 4575-4585 (2004).
27. P. Gondret and M. Rabaud, "Shear instability of two-fluid parallel flow in a Hele-Shaw cell," *Phys. Fluids* **9**, 3267-3274 (1997).
28. G. K. Batchelor, "An introduction to fluid mechanics," Cambridge University Press, New York (1967).
29. T. Cubaud and T. G. Mason, "A microfluidic aquarium," *Phys. Fluids* **19**, 091108 (2007).
30. T. Cubaud and T. G. Mason, "Formation of miscible fluid microstructures by hydrodynamic focusing in plane geometries," *Phys. Rev. E* **78**, 056308 (2008).
31. N. Rashidnia, R. Balasubramaniam and D. Del Signore, "Interfacial tension measurement of immiscible liquids using a capillary tube," *AIChE J.* **38**, 615-618 (1992).
32. R. G. Larson, "The structure and rheology of complex flluids," Oxford University Press, Inc., New York (1999).
33. A. Saugey, W. Drenckhan and D. Weaire, "Wall slip of bubbles in foams," *Phys. Fluids* **18**, 053101 (2006).
34. N. Le Grand, A. Daerr and L. Limat, "Shape and motion of drops sliding down in inclined plane," *J. Fluid Mech.* **541**, 293-315 (2005).
35. J. H. Snoeijer, G. Delon, M. Fermigier and B. Andreotti, "Avoided critical behavior in dynamically forced wetting," *Phys. Rev. Lett.* **96**, 174504 (2006).
36. C. Reudon, F. Brochard-Wyart and F. Rondelez, "Dynamics of dewetting," *Phys. Rev. Lett.* **66**, 715-718 (1991).
37. E. Rio and L. Limat, "Wetting hysteresis of a dry patch left inside a flowing film," *Phys. Fluids* **18**, 032102 (2006).